Buckling and Postbuckling Behaviour of Glare Laminates Containing Splices and Doublers. Part 1: Instrumented Tests

Ahmad S.M. Al-Azzawi[a,c,*], John McCrory[a], Luiz F. Kawashita[b], Carol A. Featherston[a], Rhys Pullin[a], Karen M. Holford[a]

[a] *Cardiff School of Engineering, Cardiff University, The Parade, Cardiff CF24 3AA, UK.*
[b] *Advanced Composites Centre for Innovation and Science (ACCIS), University of Bristol, University Walk, Bristol BS8 1TR, UK.*
[c] *College of Engineering, University of Babylon, Babylon, Iraq.*

Abstract

The progressive damage and fracture behaviour of Glare® fibre-metal laminates (FMLs) was investigated experimentally for the buckling and postbuckling regimes of laminates containing internal 'splice' and 'doubler' joints. Specimens were either 'pristine' or contained artificial delaminations in the form of strips of release film to represent manufacturing defects. Each was tested under in-plane compression. Tests were monitored using digital image correlation (DIC) for visualisation of three-dimensional full-field displacements whilst acoustic emission (AE) monitoring – combined with the novel Delta-T location algorithm – was used for the first time to detect and locate damage events in these FML structures. Results were validated using Scanning Electron Microscopy (SEM) to determine the damage mechanisms present. Large numbers of AE events were recorded at the splice and doubler locations during initial loading and throughout the postbuckling regime,

*Corresponding author. Email address: Al-AzzawiAS@cardiff.ac.uk

suggesting that the novel AE location algorithm used is suitable for the monitoring of delaminations and matrix cracks in internal features in Glare® laminates. Moreover, AE events located away from internal features correlated well with buckling and postbuckling deformation as identified by the full-field DIC data. Finally, good correlation was observed between the onset of buckling and a rapid increase in cumulative AE energy, demonstrating that as well as locating damage, AE monitoring is able to indicate quite clearly when the buckling load has been reached.

Keywords:

Glare, Buckling, Postbuckling, Delamination, Acoustic Emission, DIC, SEM

1. Introduction

Fibre-Metal Laminates (FMLs), including Glare® , are manufactured from alternating metallic sheets and fibre reinforced composite layers. Glare® , which consists of aluminium alloy sheets combined with glass fibre reinforced polymer (GFRP) layers, offers a 10% reduction in specific weight compared with monolithic aluminium and has advantages over carbon fibre reinforced polymers (CFRP) including improved impact, fire and corrosion resistance, and increased damage tolerance. Its commercial use has increased progressively and applications include the Airbus A380 fuselage, the Learjet 45, floor panels for the Boeing 737, and the cargo doors of the Boeing C-17 Globemaster III. Despite their advantages however, FMLs present additional challenges in terms of understanding the different damage mechanisms present in this class of materials. This paper examines the effects of potential damage arising from the manufacturing process, specifically from the need to introduce

joints when fabricating large panels. For a typical metal sheet of thickness between 0.3 mm and 0.4 mm the maximum width of material is normally 1.65 m, whilst a fuselage skin requires sheets of up to 2 m or wider. In order to obtain wider panels, aluminium sheets are positioned side by side with gaps in between. The gaps are staggered through the thickness to prevent loss of strength with the fibre layers providing load transfer; this is known as 'splicing'. Joints can also be strengthened by adding additional layers externally or internally to reduce stresses, and these are known as 'doublers'. Examples of both types of joints are shown in Figure 1. Although solving size restrictions, these features involve further manufacturing processes and therefore the possibility of introducing defects such as delaminations. The latter are a particular problem in structures experiencing compressive in-plane loading - and therefore subject to potential buckling.

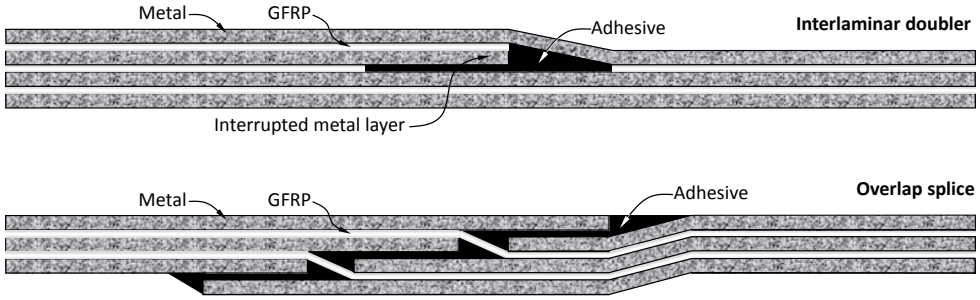

Figure 1: Schematic representations of the doubler (top) and splice (bottom) joining techniques for Glare® (adapted from [1]).

The effect of delaminations on fibre composites was studied by Clarke and Pavier [2, 3] who examined the buckling behaviour of axially loaded composite plates and found that under compressive load the presence of initial delaminations extending across the specimen's width and over 1/5 of the

specimen's length had a significant influence on their strength. Delamination growth during the buckling and postbuckling of HYE-3574 OH carbon/epoxy composites with artificial delaminations was also studied experimentally by Gu and Chattopadhyay [4]. The delamination buckling mode was found to be closely related to the location and length of the delamination. Kutlu and Chang [5] investigated the compressive response of T300/976 composite panels containing multiple delaminations. Carbon/epoxy specimens with various ply orientations were fabricated from both flat and cylindrical composite panels. Experimental results demonstrated that delamination propagation significantly affected the postbuckling response of laminated composite panels. The effect of delaminations on the postbuckling behaviour of CFRP composite laminated rectangular plates was also studied experimentally in [6]. This study found that after buckling occurs, delaminations can be expected to grow due to high interlayer shear stresses. This growth is likely to be rapid and extensive before failure. In [7] experimental and numerical studies on the buckling of GFRP laminates containing a single delamination were carried out on rectangular plates. Artificial delaminations were introduced between fabricated laminate plies using embedded rectangular fluoropolymer films of 13 μm thickness. Different fibre orientation angles were found to affect the critical buckling load, which was greatest for the 0° fibre orientation angle for all aspect ratios and widths of delamination.

Many experimental and numerical studies have been conducted in order to study the effect of delaminations on the buckling properties of composite laminates and more recently FMLs. In terms of buckling and postbuckling behaviour flat and curved fibre-metal laminate panels were first investigated

by Verolme [8, 9, 10]. Results showed that FML panels exhibited similar buckling and postbuckling behaviour to their metallic counterparts. They also emphasised the fact that the only difference was that the damage in the FMLs started with a local delamination, while the corresponding metallic panels exhibited plastic deformation. Botelho *et al.* [11] studied the compressive properties of the hybrid composites 'Glare' and 'Caral' with glass and carbon fibre composites. Results revealed that the compressive strength of composites depends on the way the loading is applied. In particular, the axial compressive strength for unidirectional polymer composites is mainly controlled by the buckling modes of the fibres [12]. The results also showed that the compressive strength was highest for CFRP laminates and lowest for FMLs mostly due to the weak interface between the composite layers and the aluminium alloy. SEM micrographs showed damage at this interface leading to buckling of the corresponding aluminium layer. Mania and York [13] studied the buckling behaviour and load carrying capacity of thin-walled FML open cross-section profiles, subject to static axial compression loading. Uni-axial compression buckling strengths obtained using semi-analytical and finite element methods were compared with experimental results. Laminate tailoring strategies, based on the use of buckling factor contours mapped onto lamination parameter design spaces were used to improve the compressive buckling load capacity for short columns of open cross-section. Kolakowski *et al.* [14] investigated the elasto-plastic buckling of FML short columns/profiles subjected to axial uniform compression. They incorporated transverse shear effects and elasto-plastic material models based on different strain-hardening plasticity theories. The work also revealed that the buck-

ling modes in the elastic and elastic-plastic range are not always identical. Kamocka and Mania [15] considered both micro and macro mechanics to study flat plates manufactured from FMLs. The properties of these specimens were determined using the Rule of Mixtures and analytical results were verified by experimental tests. After demonstrating the sensitivity of the performance of these structures to material properties, the authors highlighted the need for accurate sub-laminate material data. Frizzell *et al.* [16] performed an experimental analysis at microscopic scale to monitor the progression of damage including buckling in pin-loaded fibre metal laminates. Damage was investigated using SEM micrographs taken at different load levels up to the failure load. Different damage mechanisms were observed for instance at 90% of failure load, plastic deformation in the aluminium layers was noticed in addition to delamination at the interface between the outer aluminium layers and their adjacent 0° GFRP layers. Delamination was also noted between the 0° and 90° fibre plies with fibre kinking progressing to form micro-buckles in the 0° GFRP layers eventually leading to fibre breakage in some of these plies. Experimental studies conducted by Remmers and de Borst [17] presented delamination buckling in 'Glare 2' on a microscopic level both experimentally using Scanning Electron Microcopy (SEM) and numerically using the interface element model given by Kachanov [18]. Obdrzalek and Vrbka [19, 20] performed numerical studies on the buckling of FMLs and concluded that depending on the in-plane orientation and out-of-plane position of an artificial delamination, the buckling load can drop by up to 30% and 50% respectively. They also found that the buckling and postbuckling behaviour the plates was greatly affected by the geometrical

shape of the delamination.

Understanding the effect of geometric imperfection and load eccentricity on buckling and postbuckling behaviour of composite laminates has also been studied by many researchers. However again, comparatively less has been done to investigate the effects of such imperfections on Fibre Metal Laminates. Buckling in adhesively bonded GFRP composite flanges containing splice joints and with an initial debond were experimentally investigated by Kwon and Kim [21]. Although the flange length and width were found to affect the buckling behaviour strongly, their influence on debond growth initiation (which was seen to originate in the corners of the free edge of the buckled flange, where the highest peel stresses are found due to the postbuckled flange deformation) was only slight. The consequent growth of the debond was found to be strongly dependent on its initial length but weakly dependent on flange width [21]. Koiter [22] examined the effect of geometrical imperfections on the elastic buckling load of a cylindrical shell under uniaxial compression. This work was extended to both cylinders and spheres by Hutchinson [23] for loadings that produce biaxial membrane stresses. It was found that reducing the transverse membrane stress component leads to an increase in the axisymmetric initial imperfection (the normal deflection of the middle surface of the unloaded shell) and this behaviour is similar for both cylindrical and spherical shells. Hilburger and Starnes Jr. [24] showed that non-linear analysis can be used to determine accurate, high-fidelity design knock-down factors that can be used for predicting composite shell buckling and collapse loads in the design process. This can be achieved by considering traditional imperfections (geometric shell-wall mid-

surface imperfections) and non-traditional imperfections (shell-wall thickness variations, local shell-wall ply-gaps associated with the fabrication process, shell-end geometric imperfections, non-uniform applied end loads, and variations in the boundary conditions including the effects of elastic boundary conditions). This could be used as the basis of a generalised imperfection signature for a composite shell that includes the effects of variations or uncertainties in the shell-geometry, fabrication-process, load-distribution and boundary stiffness parameters. Tsouvalis *et al.* [25] investigated the effect of initial imperfection magnitude on the buckling loads of cylinders under external hydrostatic pressure and found a good correlation between experimental and modelling results, and Featherston [26] performed a similar study on a simple aerofoil under combined shear and in-plane bending. In [27] Hilburger reports the results of experimental and analytical studies of the effects of initial imperfections on the buckling response and failure of unstiffened thin-walled compression-loaded graphite/epoxy cylindrical shells, results that include the effects of traditional and non-traditional imperfections and uncertainties on the nonlinear response characteristics. Experimental and analytical investigations were conducted to examine the effects of the inherent mechanical couplings exhibited in fully anisotropic (*i.e.* unsymmetric) graphite/epoxy laminates on the buckling loads and mode shapes in [28]. The results indicated that these couplings, especially those which relate stretching and bending behaviour, cause out-of-plane deflections prior to buckling and hence reduce the buckling load significantly. Eglitis *et al.* [29] performed experimental and numerical studies on the buckling of concentrically and eccentrically compressed composite cylinders. Although using

values of knock-down factors which were estimated from linear eigenvalue analyses, both experimental and numerical results showed good correlation.

With respect to FMLs, the study conducted by [30] on the buckling behaviour and load carrying capacity of thin-walled FML open cross-section profiles, was extended in Mania *et al.* [31, 13] to investigate the buckling and postbuckling response of different FML profiles, with further work [32] highlighting the need to consider the effect of imperfections in order to accurately predict the consequent reduction in performance.

In this paper we extend the work of previous authors, focusing on examining the effect of delamination damage on the buckling and postbuckling characteristics of Glare® FML specimens containing two different types of joints – doublers and splices – based on a series of experiments. Specimens containing these joints have been tested under compression and monitored using Digital Image Correlation (DIC) to measure the out-of-plane displacements of the plate. Damage initiation and progression including the onset of delamination growth is detected and located using Acoustic Emission (AE) using the Delta-T algorithm presented in presented in [33] – which was designed to provide more accurate results for anisotropic materials than the previously used time-of-arrival technique to locate damage – for the first time in a fibre-metal laminate. AE event locations are compared with the full-field deformation data from the DIC data and SEM micrographs of the structure taken both remote from and within the joint to determine the level of damage and hence gain an understanding of its effect on the buckling and postbuckling behaviour of FMLs containing such joint types.

Table 1: Standard grades of commercial Glare® [1].

Grade	Sub-Grade	Alloy	Metal sheet thickness [mm]	GFRP sub-laminate layup	Main beneficial characteristics
Glare 1	-	7475-T761	0.3-0.4	0/0	fatigue, strength
Glare 2	Glare 2A	2024-T3	0.2-0.5	0/0	fatigue, strength
Glare 2	Glare 2B	2024-T3	0.2-0.5	90/90	fatigue, strength
Glare 3	-	2024-T3	0.2-0.5	0/90	fatigue, impact
Glare 4	Glare 4A	2024-T3	0.2-0.5	0/90/0	fatigue, strength (especially in 0° direction)
Glare 4	Glare 4B	2024-T3	0.2-0.5	90/0/90	fatigue, strength (especially in 90° direction)
Glare 5	-	2024-T3	0.2-0.5	0/90/90/0	impact
Glare 6	Glare 6A	2024-T3	0.2-0.5	+45/-45	shear, off-axis properties
Glare 6	Glare 6B	2024-T3	0.2-0.5	-45/+45	shear, off-axis properties

2. Experimental Setup

2.1. Specimen Design

Specimens measuring 140 mm × 80 mm (unsupported dimensions; when clamped 100 mm × 80 mm) were manufactured incorporating longitudinal splice and transverse doubler features as shown in Figure 2. These specimens were made by Airbus Germany GmbH from 0.4 mm thick sheets of aluminium alloy 2024-T3 and Hexcel S2-glass/FM94 glass fibre reinforced polymer (GFRP) unidirectional prepreg. Each GFRP 'layer' has 3 plies with the layup [90°/0°/90°] and a cured ply thickness of 0.133 mm. The layup one

side of the joint was '3/2' (three layers of aluminium and two layers of GFRP prepreg) and on the other '4/3' (four layers of aluminium and three layers of prepreg), according to the standard designation of commercial 'Glare 4B' shown in Table 1. Artificial delaminations were introduced by embedding a 4 mm wide strip of fluoropolymer film of thickness 10 μm. This artificial delamination is representative of those which could potentially be generated during manufacturing.

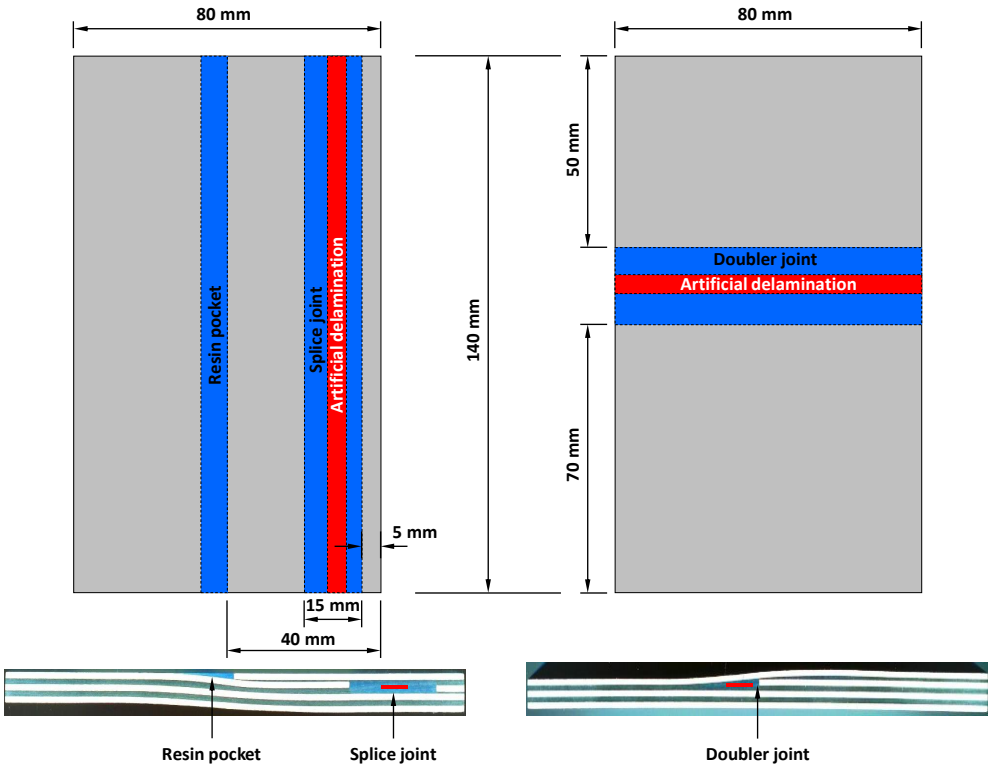

Figure 2: Layout of 'Glare 4B' specimens, (a) longitudinal splice and (b) transverse doubler.

2.2. Test Setup

The specially designed test rig seen in Figure 3, was manufactured from stainless steel 304. Specimens are held in place with four clamps. The frame was mounted in a Zwick® servo-hydraulic testing machine (fitted with a 500 kN load cell) as shown in Figure 4. The rig is designed such that when tension is applied the loading plates apply a compressive load to the specimen with axial movement of the rig being facilitated by four bronze journal bearings. The machine was operated under displacement control with a cross-head velocity of 0.1 mm $\cdot$ min^{-1}. A total of four types of specimens were tested, namely splice and doubler specimens with and without artificial delaminations, with two repeats each, totalling 8 specimens.

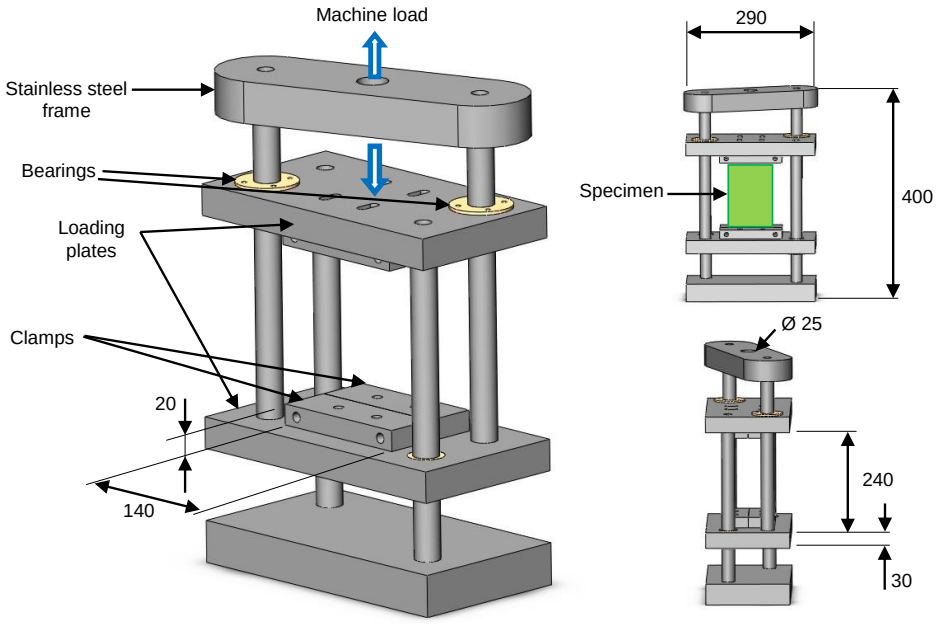

Figure 3: Buckling rig design (dimensions in mm).

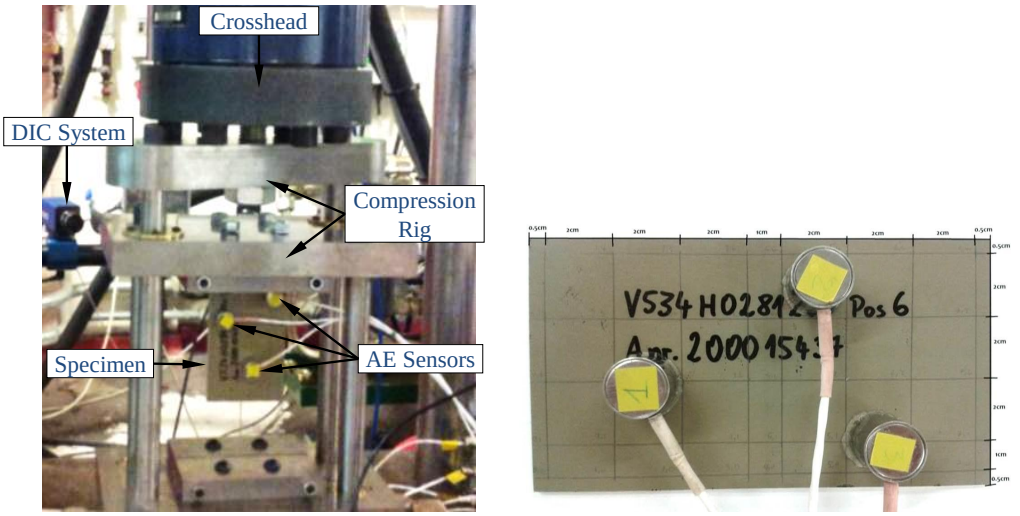

(a) (b)

Figure 4: Experimental setup (a) and position of AE sensors on the specimen (b).

3. Instrumentation

3.1. Digital Image Correlation (DIC)

Specimens were monitored using a Dantec™ Dynamics Q-400 system to record full field displacement in three dimensions to characterise the buckling and postbuckling behaviour. Specimens were prepared by applying a sprayed speckle pattern to white primed surfaces to enhance contrast. Two 2/3-inch greyscale CCD Limess™ sensors, each with a resolution of 1600×1200 pixels, were fitted with lenses of focal length 28 mm to enable a working distance of 300 mm to 600 mm. A HiLis™ monochromatic LED lighting system was used as a light source. DIC images were captured manually in approximately 1 kN steps and post-processed using the ISTRA™ 4D software with subset size 17 pixels and spatial resolution 0.2 mm.

3.2. Acoustic Emission (AE) Monitoring

Three Acoustic Emission (AE) sensors were mounted on the specimens to monitor damage events during the buckling and postbuckling regimes. The wideband sensors used in this work were supplied by Mistras™ Group and had a frequency range of 100-1000 kHz. These were chosen because they cover a wide range of waveform frequencies which enable them to detect the different types of energy produced from different materials incorporated into the Glare® laminate. These were bonded to the specimens using multi-purpose silicone sealant Loctite™ 595. The sensors were connected to a Mistras Group™ PCI2 acquisition unit with a 45 dB threshold (as recommended by previous work, including [34, 35, 36], for a wideband differential transducer) and a sampling rate of 5 MHz, recording over 1.2 ms to capture full waveforms, through pre-amplifiers with a 40 dB gain and a built-in band pass filter of 20-1200 kHz.

Event locations were calculated using a bespoke location algorithm developed at Cardiff University called 'Delta-T Mapping' [33]. The technique was developed to improve location in comparison with Time of Arrival (ToA) techniques which are based on triangulation and assume constant wave velocity in different directions, and direct paths between source and sensors. For composite structures, material anisotropy results in great variation in wave velocity with respect to in-plane direction. Moreover, for complex structures features such as holes interrupt the wave path. The Delta-T technique overcomes these limitations by mapping the structure to take these effects into account and then uses these maps in the location of any AE-generating event (impact, crack propagation).

The implementation of the Delta-T technique requires three main steps. Firstly, an area of interest is selected and marked using a regular grid system. Secondly, time of arrival data are collected at each grid node using an artificial AE source, *e.g.* pencil lead breaks. Thirdly, this ToA data is used to calculate 'Delta-T maps' for each pair of sensors (*i.e.* maps of the difference in ToA of these signals betweeneach sensor pair), which are then stored for use during the test. Finally, AE events are located by comparing the signal patterns obtained by the sensor network to the superposition of contour lines of the pre-computed Delta-T maps, resulting in accurate location data which takes into account anisotropy and any level of geometry complexity.

In the present work the Delta-T method has been applied for the first time in the monitoring of damage development in Glare® laminates. The sensitivity and accuracy of the method make it a strong candidate for the monitoring of FML structures containing anisotropic laminae [28] and internal features (such as splices and doublers) which are prone to high-cycle fatigue damage. A more comprehensive explanation of the technique can be found in [33].

3.3. Scanning Electron Microscopy (SEM)

Specimens were studied following testing using scanning electron microscopy to allow the damage mechanisms present to be identified and located. Sections were taken to enable areas both remote from and within the joints to be examined for both splice and doubler features (the locations at which these sections were taken are shown in Figures 9 and 16 for splice and doubler specimens, respectively). These sectioned specimens were finished by grinding with wet silicon carbide paper and polishing with acetone cleaner.

A carbon coating, which gives a more suitable matt finish in comparison to the alternative gold coating for metallic specimens, of 10-20 nm was applied by thermal evaporation. Specimens were then examined using a SEM type (FEI/Philips XL30 FEG ESEM). Micrographs were then taken under high vacuum using a 30 μm aperture and 20 kV accelerating voltage with a working distance of 10-12 mm between the specimens and the aperture.

4. Results and Discussion

4.1. Splice Specimen

Figures 5 and 6 show the load-displacement curves and section stress *vs.* normalised cross-head displacement curves for the splice specimens, respectively (Specimen 1 of the laminates with defects suffered from slippage in the rig and has therefore not been considered). The section stress is defined as the load divided by the cross-sectional area of the specimen, while the normalised displacement is the ratio between cross-head displacement and initial specimen length, *i.e.* $\Delta x/l_0$, where $l_0 = 100$ mm for all specimens. It should be noted that 'section stresses' are global measures and may not reflect the local stress states in each of the material constituents. Approximate 'lamina stresses' can be recovered during the initial elastic regime via the assumption of uniformity of in-plane strains. This will be discussed later in this paper, based on the material strengths provided by the accompanying paper [37].

The in-plane displacements were obtained from DIC data instead of the machine cross-head displacement as the former is believed to be more accurate (since it is not affected by the compliance of the machine). In terms of the ultimate compressive loads for the splice coupons the experimental values

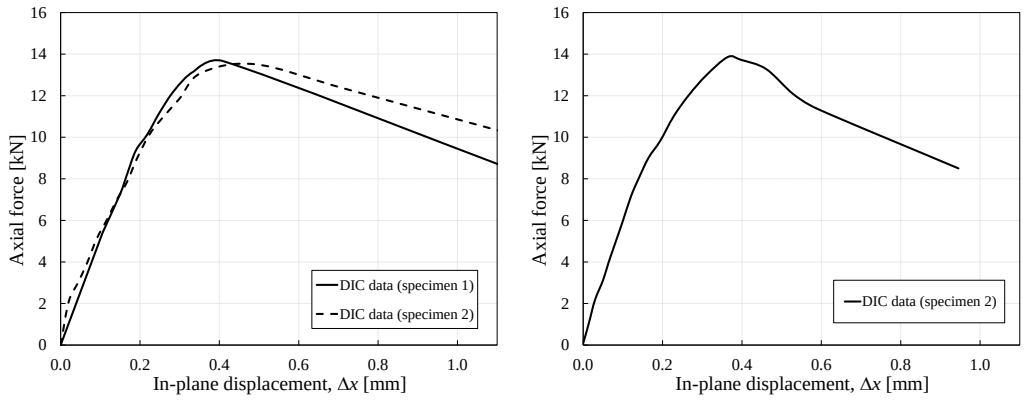

Figure 5: Axial force *versus* in-plane displacement for splice specimens; (a) pristine and (b) with an artificial defect.

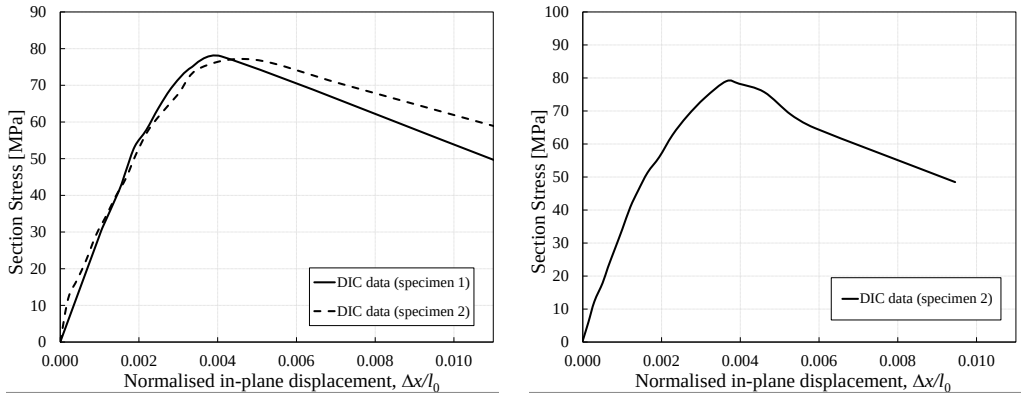

Figure 6: Section stress *versus* normalised in-plane displacement for splice specimens; (a) pristine and (b) with an artificial defect.

are 13.66 kN and 13.72 kN (corresponding to section stresses of 77.86 MPa and 78.20 MPa) with and without defects respectively. The effect of the inserted delamination on both pre and postbuckling stiffness and ultimate strength therefore appears to be negligible. This could be due to the relatively small delamination size relative to the specimen size, or the fact once global buckling has started to occur the deformation of the specimen tends to close any delamination initiated by the insertion of this localised defect which is in front of the specimens neutral axis and therefore sits between plies which are under tension during bending, which consequently has little effect on the performance of the joint under compression.

Figure 7 shows the contours of the out-of-plane displacement at initial buckling (in-plane displacement $\Delta x = 0.166$ mm), peak load ($\Delta x = 0.385$ mm) and postbuckling ($\Delta x = 0.809$ mm), obtained from DIC data. These are compared with AE location data using the Delta-T algorithm described earlier. The results presented are for splice specimens incorporating an artificial defect, but the pristine specimens presented very similar behaviour indicating that the effect of the damage introduced on the mode shape and the amplitude of out-of-plane deformations is negligible. The plate is seen to buckle with a single half wave length in the loading direction as expected for a plate with free longitudinal edges under compression. Deformations to the left of the joint in the thinner region of the specimen are higher than those to the right again as would be expected.

With respect to the AE location data in Figure 7 and cumulative AE energy in Figure 8, at approximately $\Delta x = 0.166$ mm initially low-energy AE events are detected along the horizontal centreline in an area which coincides

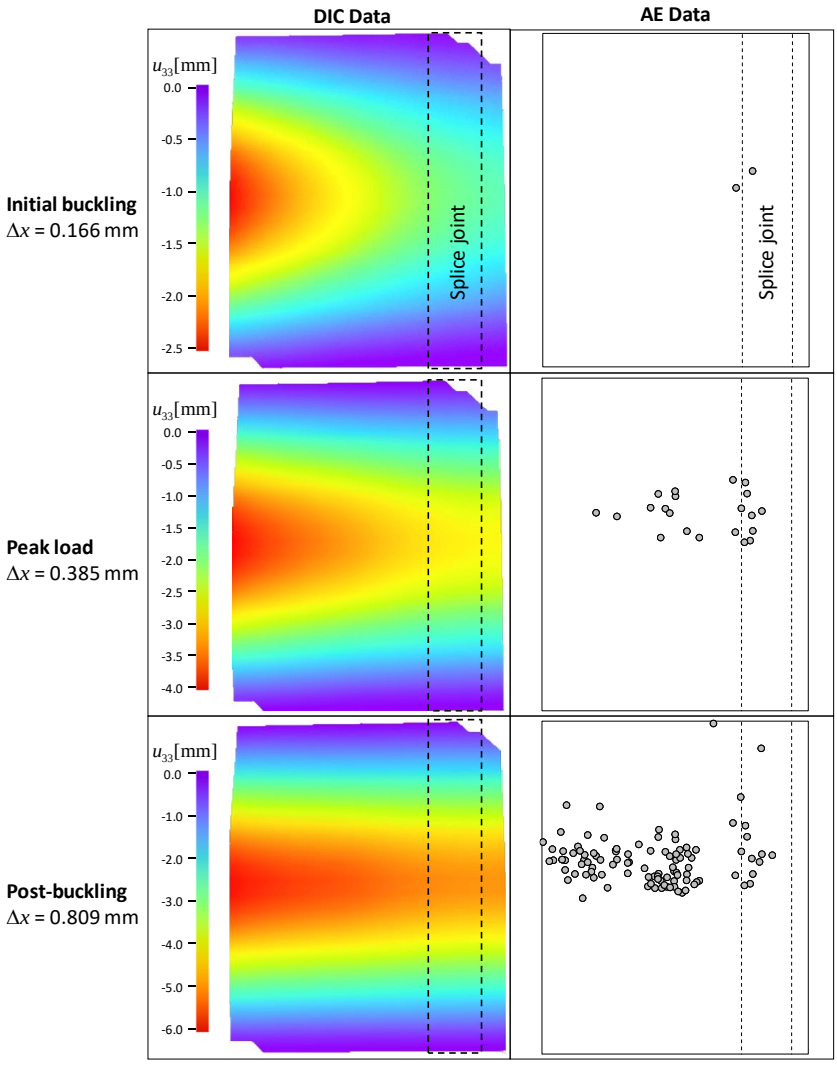

Figure 7: Contours of out-of-plane displacement (left) against location of AE events (right) for the *splice* specimen (with an artificial defect) at different in-plane displacements Δx (dashed lines indicate position of splice).

with the location of the embedded defect. This due to matrix cracking at the initial buckling load, as illustrated later by SEM micrographs (Figure 11). Then, at approximately $\Delta x = 0.385$ mm, a large number of high-energy AE

events are detected all along the centreline of the specimen where the large out of plane displacements and high curvature at the ultimate compressive load lead to further matrix cracking, as also seen in SEM micrographs (Figure 10). Further events located in the area of the splice joint correspond to widespread matrix damage leading to delamination initiation. Activity then begins to spread out along the joint at approximately $\Delta x = 0.809$ mm, indicating delamination growth in addition to shear damage in the matrix resin layers, with possible fibre breakage in 0° fibre plies. Although some level of fibre failure is expected during the postbuckling regime, only indirect observations have been made via SEM as no clear 'kink band' is observed at these moderate levels of strain. Instead, fibre failure along 0° plies appear in the form of fibres with multiple fractures along their length, *e.g.* Figure 10(b), which is likely to be a combination of fibre damage during the test with further damage during the cutting and polishing of SEM samples.

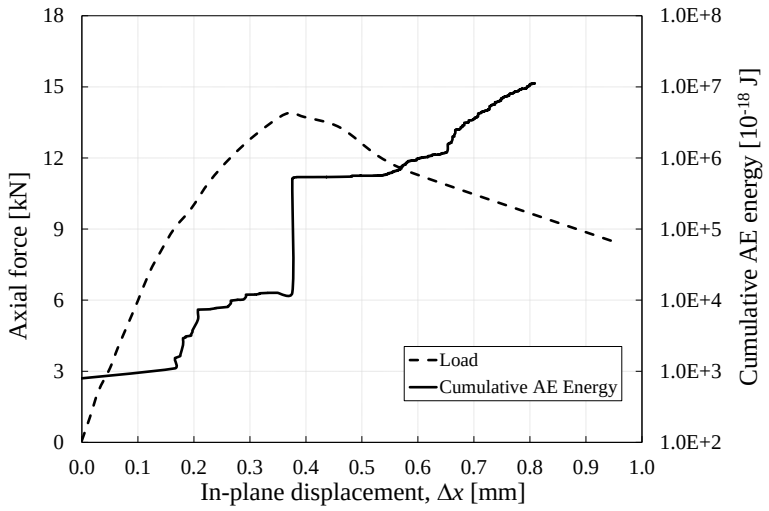

Figure 8: Load and cumulative AE energy *versus* in-plane displacement for the *splice* specimen with defect.

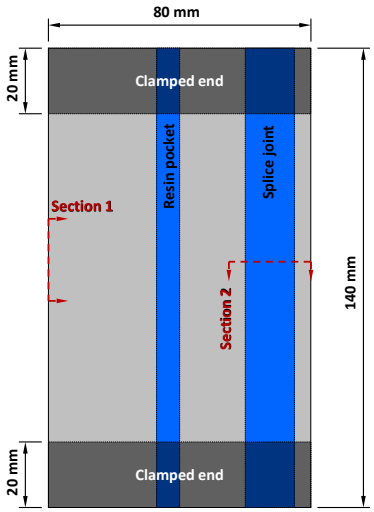

Figure 9: Sections of the *splice* specimen observed under SEM.

Figure 8 shows the cumulative energy of events occurring throughout the test period, against applied load. The first significant increase in the logarithmic cumulative energy occurs at an in-plane displacement of around $\Delta x = 0.166$ mm corresponding to matrix damage which accompanies initial buckling of the panel, indicating that AE can be used to predict the onset of buckling. A further large jump is observed when the load reaches the ultimate compressive load at $\Delta x = 0.385$ mm indicating a high level of damage activity (potentially matrix cracking and matrix shear damage, as suggested by the SEM micrographs) plus the initiation of macroscopic delamination, due to high levels of deformation and curvature at this point, as would be expected. This is followed by a gradual increase in energy which corresponds to delamination initiation and growth along the splice feature during post-buckling. Again, this interpretation is backed by the analysis of detailed nonlinear Finite Element models in [37].

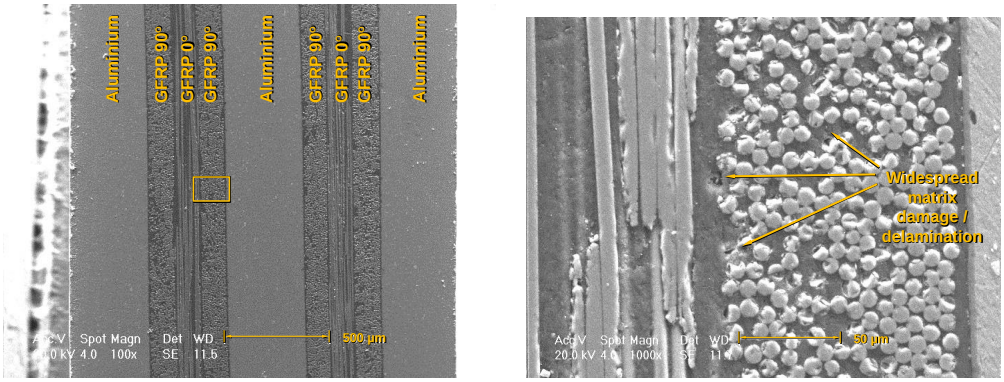

(a) (b)

Figure 10: SEM of *splice* specimens along section 1 (side of specimen), with magnifications of (a) 100× and (b) 1000×.

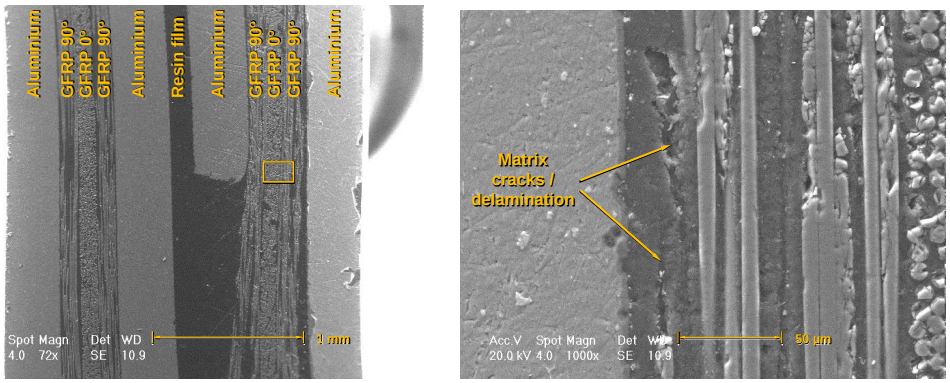

(a) (b)

Figure 11: SEM of *splice* specimens along section 2 (across splice), with magnifications of (a) 72× and (b) 1000×.

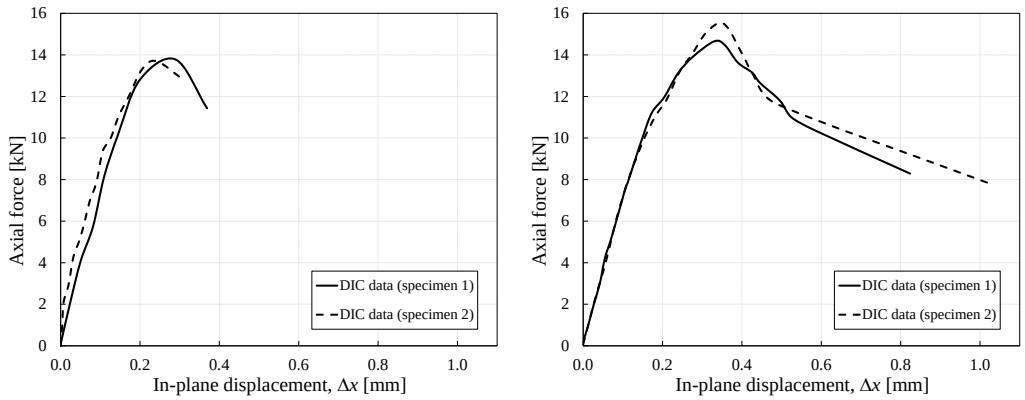

Figure 12: Axial force *versus* in-plane displacement for doubler specimens; (a) pristine and (b) with an artificial defect.

4.2. Doubler Specimen

The load *versus* in-plane displacement curves and section stress *versus* normalised displacement curves of doubler specimens with and without artificial defects are shown in Figures 12 and 13. As before, in-plane displacements were extracted from DIC data. The ultimate compressive loads for the specimens without defects are 13.78 kN and 13.69 kN (corresponding to section stresses of 85.27 MPa and 84.72 MPa) and for those with artificial defects are 14.65 kN and 15.49 kN (corresponding to stresses of 90.66 MPa and 95.85 MPa). Clearly the presence of the defect is not having any significant impact on the buckling load of the doubler specimens, and this is believed to be for the same reasons as for the splice specimens.

Using the concept of uniform strains, and utilising the material strengths presented in the accompanying paper [37], a simplified stress analysis shows that fibre damage will not occur in the 90° GFRP plies outside the joint at

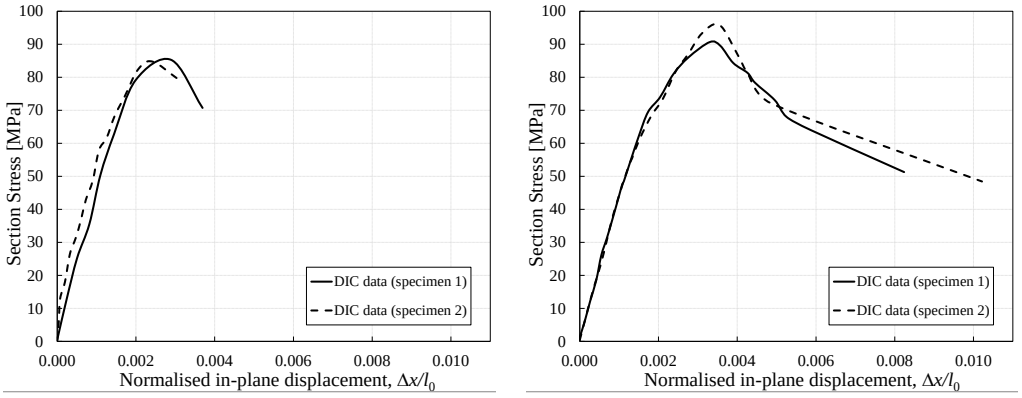

Figure 13: Section stress *versus* normalised in-plane displacement for doubler specimens; (a) pristine and (b) with an artificial defect.

peak load. Neither will matrix cracking nor shear damage between GFRP plies occur at this load for the same reason. Damage initiation is however predicted in the splice as the stresses in this thinner region are likely to exceed the ultimate normal and shear strengths for the FM94 epoxy resin.

Figure 14 shows the contours of the out-of-plane displacement for initial buckling (in-plane displacement $\Delta x = 0.173$ mm), ultimate load ($\Delta x = 0.362$ mm) and postbuckling ($\Delta x = 0.824$ mm), obtained from DIC data, which are again compared with AE event location data and AE cumulative energy (Figure 15). The results shown correspond to one of the specimens with a defect but the pristine specimens give similar results. Out-of-plane displacements can be seen to be greatest along the doubler joint, which corresponds to the panel buckling with one half wavelength along the length of the panel. It is also where a change in panel thickness occurs, with the thinner portion being above the joint. Examining the results from the acoustic

emission monitoring, Figure 14, shows initial low-energy AE events detected in the upper portion of the panel just above the doubler joint, as well as at the point of highest curvature at around $\Delta x = 0.16$ mm corresponding to the onset of buckling. This is mostly due to matrix cracking as illustrated by the SEM micrographs (Figure 18). Then, at approximately $\Delta x = 0.36$ mm when the peak load is reached, a large number of high-energy AE events are seen (Figures 14 and 15). These again correspond to the joint and the thinner section of the specimen where the out-of-plane displacements and curvatures are increasing significantly leading to matrix cracking in the resin layers as confirmed again by SEM micrographs (Figure 17). Following this point activity levels continue to increase as loading continues into postbuckling (Figure 14 particularly at the boundary of the joint with the thinner section, with the results of the SEM indicating this damage to be in the form of matrix cracking and shear damage as seen in Figure 17. In terms of AE energy the results in Figure 15 show that there is a sharp increase in cumulative energy between $0.16 \text{ mm} < \Delta x < 0.23$ mm corresponding to widespread matrix cracking. A further large jump in energy can be seen at $\Delta x = 0.36$ mm due to the large out-of-plane displacements and high curvature seen at ultimate load causing further matrix cracking. This is followed by a more gradual increase in energy up to the end of the tests at approximately $\Delta x = 0.85$ mm caused by a number of different damage mechanisms including matrix cracking and shear damage, as confirmed by SEM micrographs at the doubler joint region in Figure 18. No delamination initiation or propagation from the embedded defect was noticed in the SEM results. Again this can be explained by the fact that as the specimen begins to buckle globally, deformations act to close

any delamination which might be initiated minimising their effect. This is supported by the fact that the increase in cumulative energy is more gradual for the doubler specimen than for the splice specimen due to the smaller number of damage mechanisms which are active. This is in agreement with the Finite Element analysis presented in [37].

As also shown in Figure 14, initial low-energy AE events were detected in the upper portion of the panel just above the doubler joint, as well as at the point of highest curvature which shows great levels of AE activity at around $\Delta x = 0.16$ mm which corresponds to the onset of buckling. Then at approximately $\Delta x = 0.36$ mm a large number of high-energy AE events are seen in the same region, corresponding to the peak load when out-of-plane displacements and curvatures increase significantly.

The AE energy results shown in Figure 15 show a sharp increase in cumulative energy between 0.16 mm $< \Delta x <$ 0.23 mm corresponding to widespread matrix cracking. A further large jump in energy can be seen at $\Delta x = 0.36$ mm due again to the large out-of-plane displacements and high curvature seen at ultimate load. This is followed by a more gradual increase in energy up to the end of the tests at approximately $\Delta x = 0.85$ mm. The increase in cumulative energy is more gradual for the doubler specimen than for the splice specimen. This suggests that the transverse doubler joint investigated here does not promote large scale delaminations as observed for the longitudinal splice joint. This is supported by the detailed Finite Element analysis presented in [37].

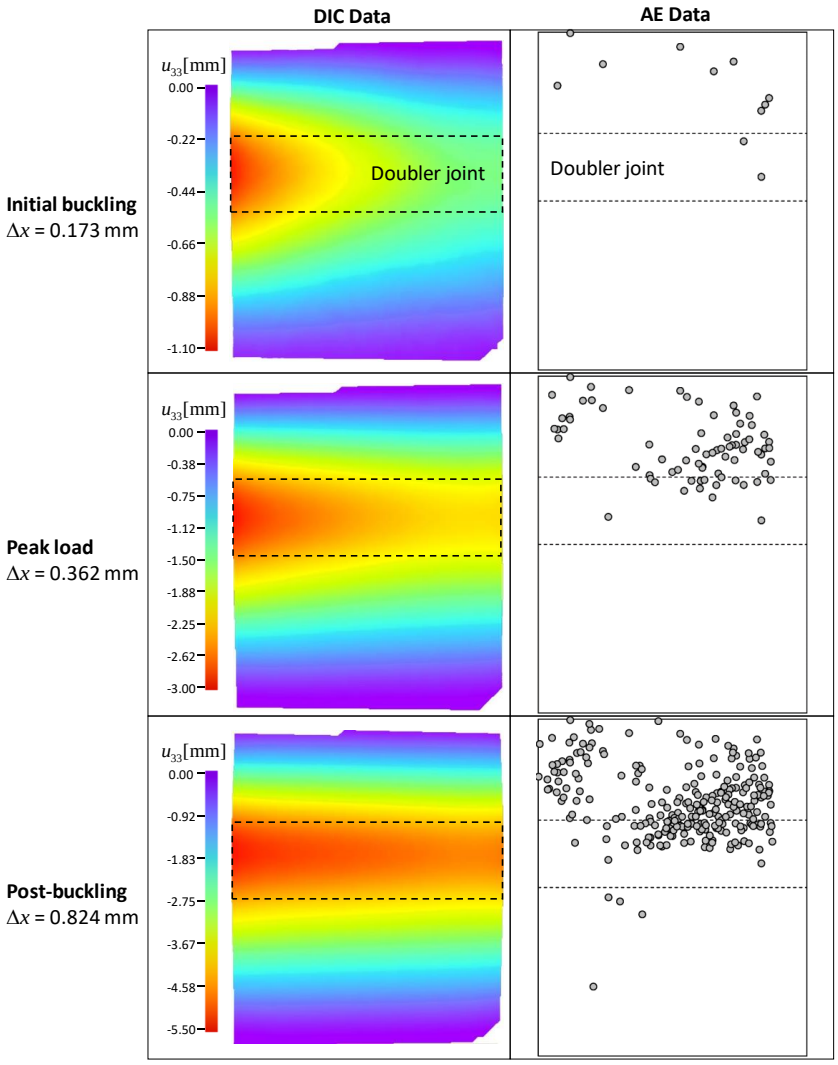

Figure 14: Contours of out-of-plane displacement (left) against location of AE events (right) for the *doubler* specimen (with an artificial defect) at different in-plane displacements Δx (dashed lines indicate position of doubler).

5. Conclusions

A series of experiments was performed to examine the effect of splice and doubler joints on the buckling and postbuckling behaviour of Glare®

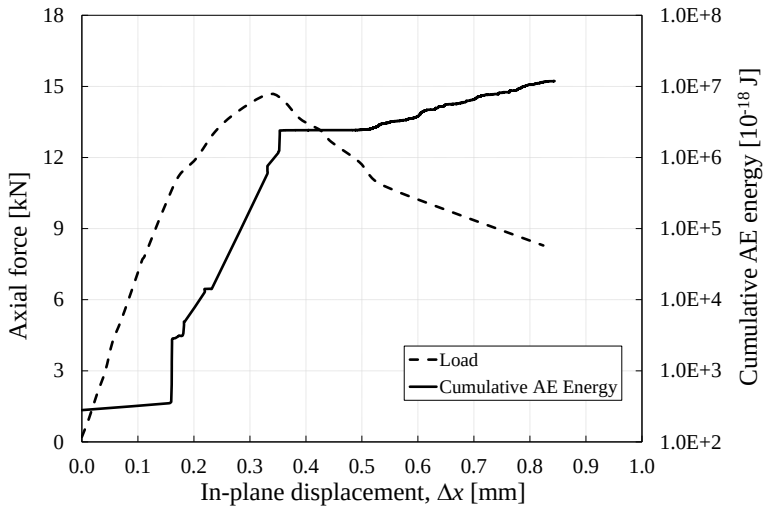

Figure 15: Load and cumulative AE energy *versus* in-plane displacement for the *doubler* specimen with defect.

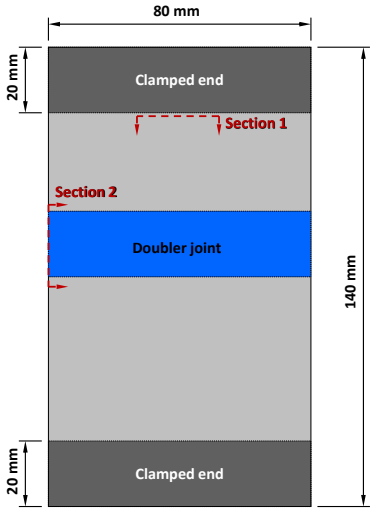

Figure 16: Sections of the *doubler* specimen observed under SEM.

fibre-metal laminate specimens containing internal splice and doubler joints. Panels were tested under in-plane compression with and without the introduction of artificial defects. Tests were recorded using Digital Image Corre-

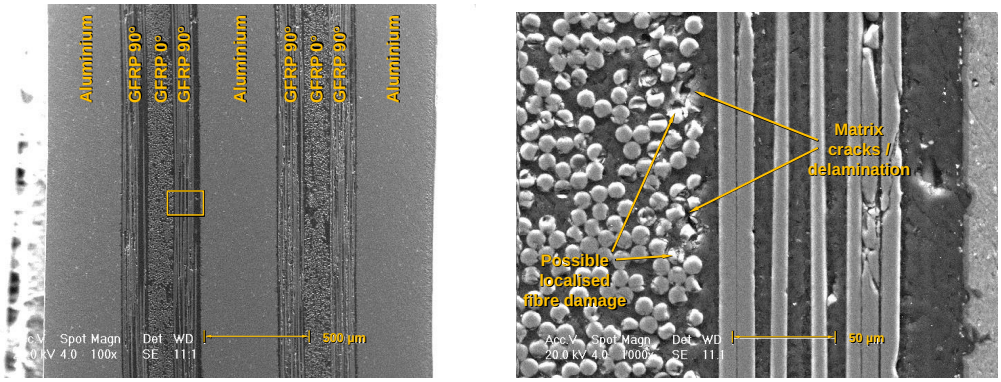

(a) (b)

Figure 17: SEM of *doubler* specimens along section 1 (near the top grip), with magnifications of (a) 100× and (b) 1000×.

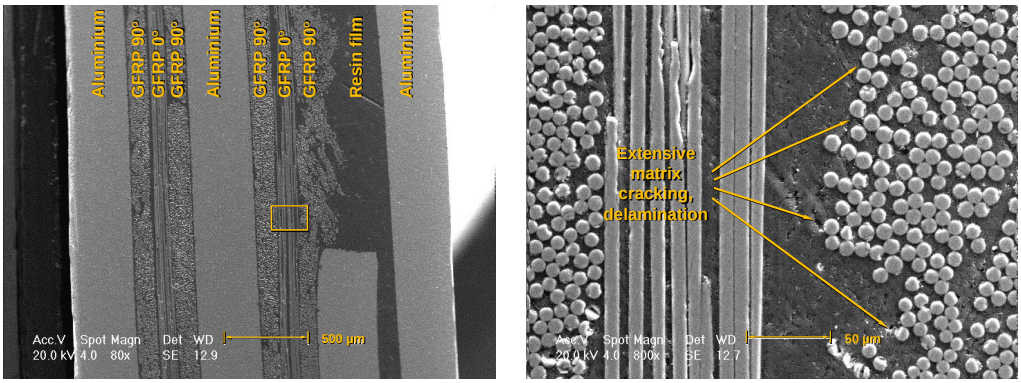

(a) (b)

Figure 18: SEM of *doubler* specimens along section 2 (across doubler), with magnifications of (a) 80× and (b) 800×.

lation (DIC) and Acoustic Emission (AE) monitoring systems. A bespoke Delta-T algorithm was implemented for accurate detection and location of damage from the recorded AE signals. Good correlation was observed between in-plane loads, out-of-plane displacements and AE event location which suggest that the postbuckling behaviour of both joints involves different damage mechanisms. The longitudinal splice joint did not promote early matrix cracking and the buckling point was characterised by a greater amount of delamination, as seen by a large jump in cumulative AE energy and the sudden increase in out-of-plane displacements. The transverse doubler joint on the other hand showed a much more gradual damage behaviour during postbuckling, dominated by widespread matrix cracks. The 'Delta-T ' AE location algorithm was successfully used to monitor damage development in the Glare® laminates. The location and sequence of AE events suggest that the method is particularly sensitive to early activity within the internal features which act as stress concentrations. Artificial delaminations representative of those which could potentially be generated during manufacturing had a negligible effect on the compressive strength of both types of joints; yet the Delta-T algorithm was able to detect their presence at relatively low loads, suggesting that the method is a strong candidate for the in-service Structural Health Monitoring of Glare® structures.

6. Acknowledgements

The authors would like to thank Iraqi Ministry of higher education and scientific research for supporting this research and Airbus Germany GmbH for the specimens and the technical staff of Cardiff School of Engineering for

their kind assistance with the testing programme.

7. References

[1] J. W. Gunnink, A. D. Vlot, Fibre Metal Laminates - An Introduction, Kluwer Academic Publishers, 2001. doi:10.1007/978-94-010-0995-9. URL http://www.springer.com/gp/book/9781402000386

[2] M. Clarke, M. Pavier, Artificial damage techniques for low velocity impact in carbon fibre composites, Composite Structures 25 (1-4) (1993) 113–120. doi:10.1016/0263-8223(93)90157-L.

[3] M. Pavier, M. Clarke, Experimental techniques for the investigation of the effects of impact damage on carbon fibre composites, Composites Science and Technology 55 (1995) 157–169. doi:10.1016/0266-3538(95)00097-6.

[4] H. Gu, A. Chattopadhyay, An experimental investigation of delamination buckling and postbuckling of composite laminates, Composites Science and Technology 59 (6) (1999) 903–910. doi:10.1016/S0266-3538(98)00130-4.

[5] Z. Kutlu, F.-K. Chang, Composite panels containing multiple through-the-width delaminations and subjected to compression. Part I: Analysis, Composite Structures 31 (1995) 273–296. doi:10.1016/0263-8223(95)00092-5.

[6] M. Aslan, W. Banks, The effect of multiple delamination on postbuck-

ling behavior of laminated composite plates, Composite Structures 42 (1998) 1–12. doi:10.1016/S0263-8223(98)00040-3.

[7] Y. Pekbey, O. Sayman, A numerical and experimental investigation of critical buckling load of rectangular laminated composite plates with strip delamination, Journal of Reinforced Plastics and Composites 25 (7) (2006) 685–697. doi:10.1177/0731684406060566.

[8] K. Verolme, Crippling and short-column buckling of fiber metal laminates, Tech. rep., Delft University of Technology (1994).

[9] K. Verolme, The initial buckling behavior of flat and curved fiber metal laminate panels, Tech. rep., Delft University of Technology (1995).

[10] K. Verolme, The development of a design tool for fiber metal laminate compression panel, Ph.D. thesis, Delft University of Technology (1995).

[11] E. C. Botelho, R. A. Silva, L. C. Pardini, M. C. Rezende, A review on the development and properties of continuous fiber/epoxy/aluminum hybrid composites for aircraft structures, Materials Research 9. doi:10.1590/S1516-14392006000300002.

[12] D. Hull, T. Clyne, An Introduction to Composite Materials, Cambridge University Press, 1996.

[13] R. J. Mania, C. Bronn, Buckling strength improvements for fibre metal laminates using thin-ply tailoring, Composite Structures 159 (2017) 424–432.

[14] Z. Kolakowski, K. Kowal-Michalska, Static buckling of fml columns in elastic-plastic range, Mechanics and Mechanical Engineering 20 (2) (2016) 151–166.

[15] M. Kamocka, R. J. Mania, Analytical and experimental determination of fml stiffness and strength properties, Mechanics and Mechanical Engineering 19 (2) (2015) 141–159.

[16] R. Frizzell, C. McCarthy, M. McCarthy, An experimental investigation into the progression of damage in pin-loaded fibre metal laminates, Composites Part B: Engineering 39 (6) (2008) 907–925.

[17] J. Remmers, R. de Borst, Delamination buckling of fibre-metal laminates, Composites Science and Technology 61 (2001) 2207–2213. doi:10.1016/S0266-3538(01)00114-2.

[18] L. M. Kachanov, Delamination buckling of composite materials, Kluwer Academic Publishers, 2001. doi:10.1007/978-94-009-2819-0.

[19] V. Obdrzalek, J. Vrbka, On buckling of a plate with multiple delaminations, Engineering Mechanics 17 (1) (2010) 37–47.
URL www.engineeringmechanics.cz

[20] V. Obdrzalek, J. Vrbka, On the applicability of simple shapes of delaminations in buckling analyses, Composites Part B: Engineering 42 (3) (2011) 538–545. doi:10.1016/j.compositesb.2010.11.006.

[21] H. Kwon, H. Kim, Buckling and debond growth of partial debonds in adhesively bonded composite splice joints, Composite Structures 79 (2007) 590–598. doi:10.1016/j.compstruct.2006.02.021.

[22] W. Koiter, The effect of axisymmetric imperfections on the buckling of cylindrical shells under axial compression, Proc Koninklijke Nederlandse Akademie van Wetenschappen (1963) 265–279.

[23] J. Hutchinson, Knockdown factors for buckling of cylindrical and spherical shells subject to reduced biaxial membrane stress, International Journal of Solids and Structures 47 (2010) 1443–1448. doi:10.1016/j.ijsolstr.2010.02.009.
URL https://dash.harvard.edu/handle/1/4215082

[24] M. Hilburger, J. Starnes, Effects of imperfections on the buckling response of compression-loaded composite shells, International Journal of Non-Linear Mechanics 37 (2002) 623–643. doi:10.1016/S0020-7462(01)00088-9.

[25] N. Tsouvalis, A. Zafeiratou, V. Papazoglou, The effect of geometric imperfections on the buckling behaviour of composite laminated cylinders under external hydrostatic pressure, Composites: Part B 34 (2003) 217–226.

[26] C. A. Featherston, Experimental buckling of a simple aerofoil under combined shear and in-plane bending, Journal of Mechanical Engineering Science 218 (2) (2004) 155–172. doi:10.1243/095440604322886919.

[27] M. Hilburger, J. Starnes, Effects of imperfections of the buckling response of composite shells, Thin-Walled Structures 42 (2004) 369–397.

[28] M. Eaton, R. Pullin, K. Holford, Acoustic emission source location in composite materials using Delta-T mapping, Composites Part A:

Applied Science and Engineering 43 (2012) 856–863. doi:10.1016/j.compositesa.2012.01.023.

[29] E. Eglitis, K. Kalnins, O. Ozolinsh, The influence of loading eccentricity on the buckling of axially compressed imperfect composite cylinders, Mechanics of Composite Materials 46 (5) (2010) 483–492.
URL http://dx.doi.org/10.1007/s11029-010-9165-7

[30] R. J. Mania, Comparative static buckling study of fml thin-walled profiles, in: ECCM16 16th European conference on composite materials, Sevilla, Spain, 2014.
URL http://www.eccm16.org

[31] R. J. Mania, Z. Kolakowski, J. Bienias, P. Jakubczak, K. Majerski, Comparative study of fml profiles buckling and postbuckling behaviour under axial loading, Composite Structures 134 (2015) 216–225.

[32] D. Banat, Z. Kolakowski, R. Mania, Investigations of FML profile buckling and post-buckling behaviour under axial compression, Thin-Walled Structures 107 (2016) 335–344.

[33] M. Baxter, R. Pullin, K. Holford, S. Evans, Delta T source location for acoustic emission, Mechanical Systems and Signal Processing 21 (2007) 1512–1520. doi:10.1016/j.ymssp.2006.05.003.

[34] O. Büyüköztürk, M. A. Tademir, Nondestructive testing of materials and structures, Springer New York, 2013.

[35] M. R. Pearson, Developement of lightweight structural health monitoring systems for aerospace applications, Ph.D. thesis, Cardiff University (2013).

[36] S. Al-Jumaili, Damage assesment in complex structures using Acoustic Emission, Ph.D. thesis, Cardiff University (2016).

[37] A. Al-Azzawi, L. Kawashita, C. Featherston, Buckling and post-buckling behaviour of glare laminates containing splices and doublers. Part 2: Numerical modelling, *manuscript submitted to* Composite Structures.